VARIATIONS IN VENUS CLOUD-PARTICLE PROPERTIES: A NEW VIEW OF VENUS'S CLOUD MORPHOLOGY AS OBSERVED BY THE GALILEO NEAR INFRARED MAPPING SPECTROMETER

by

R. W. Carlson[1], L. W. Kamp[1], K. H. Baines[1], J. B. Pollack[2], D. H. Grinspoon[3], T. Encrenaz[4], P. Drossart[4], and F. W. Taylor[5]

[1]Jet Propulsion Laboratory, California Institute of Technology, Pasadena, California 91109

[2]Ames Research Center, National Aeronautics and Space Administration, Moffet Field, California 94035

[3]University of Colorado, Boulder, Colorado 80309

[4]Observatoire de Paris, 92195 Meudon, France

[5]Oxford University, Oxford OX1 3PU, United Kingdom

Submitted to Planetary and Space Science

March, 1993

ABSTRACT

Using Venus nightside data obtained by the *Galileo* Near Infrared Mapping Spectrometer, we have studied the correlation of 1.74 and 2.30 μm radiation which is transmitted through the clouds. Since the scattering and absorption properties of the cloud particles is different at these two wavelengths, one can distinguish between abundance variations and variations in the properties of the cloud particles themselves. The correlation of intensities shows a clustering of data into five distinct branches. Using radiative transfer calculations, we interpret these branches as regions of distinct but different mixes of Mode 2' and 3 particles. The data and calculations indicate large differences in these modal ratios, the active cloud regions varying in content from nearly pure Mode 2' particles to almost wholly Mode 3. The spatial distribution of these branches shows large scale sizes and both hemispheric symmetries and asymmetries. High latitude concentrations of large particles are seen in both hemispheres and there is banded structure of small particles seen in both the north and south which may be related. The mean particle size in the northern hemisphere is greater than found in the south. If these different branch regions are due to mixing of vertically stratified source regions (e.g. photochemical and condensation source mechanisms) then the mixing must be coherent over very large spatial scales.

INTRODUCTION

A large body of evidence, based upon *Pioneer, Venera,* and *Vega* probes, indicates that the clouds of Venus are vertically stratified, with three main cloud layers identified. The uppermost cloud layer, the "Upper cloud", is that level generally seen in visible remote-sensing and tends to be a uniformly opaque and featureless cloud layer, exhibiting contrasts which are observable mainly in the ultraviolet region. This, and the underlying "Middle" and "Lower" clouds are characterizations derived from in-situ measurements of particle densities and sizes (Knollenberg and Hunten, 1979, 1980). Prior to the discovery of the near infrared windows in the Venus spectrum by Allen and Crawford (1984), the Middle and Lower clouds were unobserved by remote sensing techniques.

In addition to this vertical stratification, these cloud layers appear to possess at least three different particle-size components, referred to as modes: Mode 1 particles, present in the Upper Cloud and, at lesser relative concentration, also in the Middle and Lower Cloud regions, are sub-micron size particles with average diameters of approximately 0.6 *pm*. Modes 2 and 2' particles are larger, with mean diameters of roughly 2 and 3 μm respectively. Mode 2 particles occur in the Upper Cloud and produce the dominant optical opacity in that region, while the slightly larger Mode 2' particles are present in the Lower and Middle Clouds. These bottom two regions (Middle and Lower Clouds) also exhibit the large Mode 3 particles, with average diameter of 7 *pm*. A summary of Venus cloud properties is given in Esposito et al. (1983).

This simplified scheme of vertical stratification and size parameterization attempts to describe the global and time-averaged properties of the Venus clouds. However, the various probe data show considerable differences in these cloud properties, indicating that there are spatial and/or temporal variations occurring as well. In particular, the *Pioneer Venus* nephelometer experiments (Ragent and Blamont, 1980) sampled four widely separated sites, finding large differences at Lower Cloud levels from one site to another. In contrast, the higher (Middle Cloud) regions were found to be nearly identical in scattering properties for all four locations. Similar indications of variability at lower levels were obtained by the nephelometers on the *Venera 9, 10, and 11* probes. (Marov et al., 1980). A comparison of *Pioneer Venus* particle size spectrometer data (Knollenberg and Hunten; 1979, 1980) with those from the two *Vega* spectrometers (Moshkin et al., 1986) shows considerable differences in the large particle abundances at the bottom cloud levels, with the *Vega* data indicating an absence of large particles where the *Pioneer* data show large abundances, Spatial and temporal variations in cloud opacity have been observed in ground-based (Crisp et al., 1989) and *Galileo* (Carlson et al., 1991) infrared images and these opacity variations have been attributed to changes occurring in the lower cloud regions (Crisp et al., 1986; Carlson et al., 1991; Grinspoon et al., 1993 this issue). For images obtained at a single wavelength one can merely sense opacity changes; with multiple wavelengths one can distinguish between changes in abundance and changes in the cloud particles. In this paper we use high spatial resolution images obtained at two wavelengths

to discern the spatial variations of cloud particles properties (for a particular instant in time).

The source of these data is the Near Infrared Mapping Spectrometer Experiment NIMS (Carlson et al., 1992) and they were obtained during the February 1990 *Galileo* flyby of Venus. During this flyby, NIMS imaged the nightside of Venus in seventeen spectral channels, from the visible (0.8 *pm)* to the thermal infrared (5.2 μm). *The* longer wavelength channels are useful for probing the upper cloud regions and their corresponding thermal emission properties (see the accompanying papers by Roos et al. 1993 and Grinspoon et al., 1993). At shorter wavelengths, there is less absorption by cloud particles and the clouds become translucent. This allows thermal emission produced below the clouds to be observed in transmission, and images of this transmitted radiation can show spatial variations in cloud properties,

In the work presented here, we utilize the well-known spectral windows at 2.30 μm and 1.74 μm, which were imaged simultaneously by NIMS during the February 1990 Venus Encounter. These measurements are briefly described in Carlson et al. (1991). The images at both of these wavelengths show similar patterns of cloud structure, but with differing amounts of contrast. The contrast at 2.30 μm is -20:1, whereas the corresponding 1.74 μm value is $\sim$ 5:1. It is reasonable to associate these contrast differences with the wavelength-dependent scattering and absorption properties of sulfuric acid cloud particles, known to exist in the Venus clouds. In particular, these particles are more absorbing at 2.30 μm than at 1.74 μm, *so* multiple scattering events will produce more net absorption and therefore more contrast for the longer wavelength radiation.

Assuming the correctness of the above assertion - that the contrasts are due to cloud particle characteristics - then a useful tool to study the properties of the Venus clouds is a comparison of the 1.74 and 2.30 μm radiances, sometimes referred to as a scatter or correlation plot. This method was used in our preliminary analysis (Carlson et al., 1991), where it was found that the relationship between intensities, i.e. $I_{1.74}$ vs. $I_{2.30}$, showed two different curves or "branches". These two branches were found to correspond to a north-south hemispherical asymmetry, along with a linear feature, occurring at -45 N and with a northerly slope (as seen by a co-rotating observer).

In this work, we extend this line of investigation, finding additional branches. The spatial distribution of these branches is investigated and compared to images of cloud extinction and cloudtop thermal emission. In an attempt to find a physical basis for the different branches, we then investigate the specific shape of individual branch curves using radiative transfer calculations.

VENUS CLOUD BRANCHES

In our earlier and preliminary work, we used a rudimentary method to assign data values to individual image pixels and did not take into account the spatial response profile of the instrument. Furthermore, the scatter plot analysis used data from a limited amount of the observed disc. In this work, we use a more accurate description of the instrumental response and include more observed points.

In addition, we have found that a correction for emission angle is necessary for radiances near the limb. To do so, we have used the radiative transfer model of Kamp and Taylor (1990) to find the theoretical variation of radiance with emission angle for a nominal cloud model developed by Pollack et al. (1993). These calculations use 21 angular points per hemisphere, and were monochromatic at the NIMS band center wavelengths (1.74 and 2.30 μm). Test were performed which show that the results are essentially unchanged over the NIMS bandpasses, so the monochromatic assumption is not expected to introduce significant error. It can be seen in Fig. 1 that the results follow reasonably well the upper envelope of the observational data, which can be expected to define a locus of points for a given cloud thickness (i.e. the optically thinnest cloud in the observation). The theoretical values at low values of $\cos(\theta_e)$ are not to be trusted due to the breakdown of the plane-parallel assumption at these steep zenith angles; e.g. the upturn in Fig. lb is probably spurious.

The dashed curves in Fig. 1 are linear approximations to the model curves shown, and were used to generate the emission-angle-corrected radiances I' shown below. The equ ations for the corrected radiances (indicated by a prime) are

$$I'_{1.74} = I_{1.74}\,[\,0.316 + 0.685\,\cos\theta_e\,]^{-1}$$
$$I'_{2.30} = I_{2.30}\,[\,0.232 + 0.768\,\cos\theta_e\,]^{-1} \qquad (1)$$

The scatter plots generated using the above corrections are shown in Fig. 2a and 2b. The corrected intensities I' are shown on a linear scale in Fig 2a which best resolves the branching behavior at high radiances. The branching behavior at low intensities is better shown in the logarithmic presentation (Fig. 2b). A visual inspection of these two figures clearly shows the existence of several distinct branches. There are four obvious branches, indicating at least four distinct types of behavior. We will show below that there are in fact five branches, which are called out in Fig. 2a, although branches 4 and 5 are not well resolved in this presentation.

In order to quantify this branching behavior and study its spatial structure, we have defined the following empirical quantity D:

$$D = log_{10}(I'_{1.74}) - m\, log_{10}(I'_{2.30}) - DO \qquad (2)$$

where $m\, log_{10}(I'_{2.30}) + DO$ represents a straight line running through the center of the data in the logarithmic plot, Fig. 2b. Here, m is the slope of this line ($m = 0.53$), and DO is an arbitrary constant that determines the scaling of D. A value of D is computed for each observed point $(I'_{2.30}, I'_{1.74})$, which measures its distance above or below this reference line. A tendency for points to cluster along a branch will be evident by the occurrence of preferred values of D.

Histograms of D for two different regions over the surface are shown in Fig. 3. The top panel of Fig. 3 corresponds approximately to the upper third of the observed disc, while the lower panel describes the bottom two-thirds. With this twofold division, five maxima are evident in these distributions, indicating five branches. The maximum which is labeled 1 and occurs at a bin number of 70 in the upper histogram corresponds to the uppermost branch in Fig. 2. The other histogram peaks likewise follow the numbering scheme shown in Fig. 2a.

The histogram assigned as Number 2 may be a double, however this bifurcation is difficult to establish with certainty. The widths of the histograms are fairly large compared to the distance between adjacent maxima. Nevertheless, they show that the clouds of Venus are segregated into several distinct sets of cloud particle properties.

A false-color image of the spatial distribution of the branching parameter D is shown in Fig. 4a. It is repeated, with a superimposed latitude-longitude grid, in Fig. 4d. Also shown for comparison are maps related to the 2.30 μm cloud opacity and 4.56 μm thermal emission from the cloud tops. The color coding of the branching distribution varies from magenta (for large D values, i.e. the upper branch in Fig. 2.) to blue (corresponding to small d values and the lowest branch in Fig. 2).

The five branches, previously identified in the scatter plots and histograms, are located as follows: Branch 1 is the magenta colored area centered at 60 deg N and extending from the left side of the observed disc to ~ 330 W longitude. This branch is surrounded by the possibly double branch number 2, shown as orange and yellow. Immediately south of these two branches is a linear feature, appearing green and corresponding to Branch number 4. This linear band shows definite spatial structure, exhibiting central streaks of differently behaving material. To the south of this band is Branch number 3, shown as the gold/brown area. Below this is the hemispherically sized green/blue region corresponding to Branch number 5, which may actually be composed of several narrower histogram peaks that merge together when superimposed. (This structure emerges when histograms are constructed for smaller spatial regions.) The boundaries between the various regions show varying degrees

of sharpness. The transition between Branches 1 and 2 is fairly gradual whereas the boundaries of branch regions 3 and 4 are more sharply defined.

The general trend of the branch distribution is for the upper branches to occur in the northern hemisphere, with the lowest branch Occurring in the southern hemisphere. This hemispherical asymmetry is consistent with our earlier finding (Carlson et al.,1991). The northern hemisphere shows the greatest amount of discrete branching variation; the southern hemisphere shows a fairly continuous variation, except for the appearance of a higher branch in the southern polar region. This latter feature may be an artifact due to incorrect emission angle corrections. However other regions along the limb, for which the emission angle is the same, do not exhibit such behavior. If this is indeed a true feature, then there is possible hemispherical symmetry in the high latitudes, with high values of the branching parameter occurring poleward of ~50 deg north and south latitude. Another possible symmetry is the suggestive correspondence of the 45 N linear structure with a set of weak linear streaks occurring in approximately the same southern latitude region. This *is* reminiscent of the bow shaped bands seen in spacecraft imagery (cf. Rossow et al. 1980) and explained by Schinder et al. (1990) as streamlines.

The spatial scales of the individual branch regions are quite large. A typical longitudinal width is of order 5 - 15 degrees, or 500- 1500 km. The latitudinal extent for many of the regions is at least one quarter of the planetary circumference, or >10,000 km.

It is of interest to compare this branching map with a corresponding map of cloud extinction which is shown in Fig. 4b. This "extinction map" is simply the radiance levels at 2.30 μm, so high extinction appears dark. There are some obvious correlations, particularly for the streaks in the southern hemisphere. Correlations in the northern hemisphere are less obvious. The low latitude boundary of the Branch 3 region (e.g. at 15 deg N) correlates with a cloud brightness boundary, and the center of this region (at zero deg longitude, 25 deg N) corresponds to a very dark area in the 2.30 μm image. The northern hemisphere linear structure which is evident in both images appears to be related, but not in an obvious fashion.

Also shown in Fig. 4C is a cloudtop thermal emission map, obtained at a wavelength of 4.56 *pm*. There may be a small amount of correlation in the region of the 45 N linear feature and elsewhere, although the structure in the thermal map is quite diffuse and correlations are difficult to establish. Since the observed 4.56 μm emission originates far above the level which produces the near infrared contrasts, little correlation is expected.

SUGGESTED INTERPRETATION OF THE BRANCHES

In this section we attempt to explain the cloud properties which influence the transmission properties of the clouds and produce the different curves (branches) shown in Fig, 2. In particular, we explore the simplest explanation, considering the effect of particle size on the transmission at the two wavelengths of interest. The changes in cloud extinction have been

shown to occur in the bottom few km of the cloud deck (see Carlson et al., 1991 and Grinspoon et al., 1993, this issue) where most of the infrared opacity is largely due to mode 2' and mode 3 particles. We therefore examine the effect of variable proportions of these two populations only; we can derive very little information about mode 1 particles since their influence on infrared transmission variations is minimal.

Based upon Mie scattering calculations it is found that the ratio of optical depths $\tau_{1.74}/\tau_{2.30}$ is greater for the mode 2' particles, compared to the larger mode 3 particles, Thus, for a given 2.30 μm radiance, the 1.74 radiance will be less for a cloud of mode 2' particles than for a cloud of mode 3 particles. This suggests that the upper branches contain more of the larger size particles than the lower branches.

We can sharpen this rough argument by performing radiative transfer calculations. This was done using the radiative transfer method of Kamp and Taylor (1990), which includes Mie scattering and uses a difference-equation algorithm. Fig. 5 shows the computed relationship between the two radiances, for three cloud cases, one consisting of only mode 2' particles, one consisting of only mode 3 particles, and the intermediate case of a mixture, with roughly equal 2.30 μm opacities for both modes. Comparison of Fig. 5 and Fig. 2a shows considerable similarity, encouraging us to explore this suggestion and compare theoretical calculations with the observed values.

For these quantitative comparisons, we start with an accurate cloud model of Venus, previously developed by Pollack et al. (1993) to represent the average properties of the Venus atmosphere as observed in ground-based spectroscopic measurements. Starting with this reference model, we vary the total optical depth of the lower cloud, but maintain constant proportions of mode 2' and mode 3 particles. Using this variable opacity, we compute radiances at the wavelengths of interest. Their relationship is shown as the center, solid curve in Fig. 6a and 6b. We then consider deviations from this reference cloud model. Two cases of relative mode concentrations are considered: either an enhancement or depletion of the relative abundance of mode 3 particles, relative to mode 2', by a factor of approximately five in each case. This enhancement/depletion is considered for another two conditions: they either occur within the lower cloud only, or within both the lower and middle clouds taken together. In each case, it is only the lower cloud that is allowed to vary in opacity. The two cases of enhancement/depletion and the two cases of lower-cloud only/lower-plus-middle-cloud yield four additional curves, shown on Fig. 6a and 6b. The normalization of these calculations is somewhat arbitrary, depending upon the extinction in the upper cloud. However, this is unimportant for the points made below.

For comparison to experimental data, we show these five cases along with a scatter plot for a single branch, number 4, (Fig. 6a) and for all of the branches (Fig. 6b). The single-branch behavior illustrated in Fig. 6a indicates that, even though there is a large variation in optical depth, the proportion of mode 3 particles to mode 2' is relatively constant, This conclusion was also found in an independent study by Grinspoon et al. (1993, this issue) who have analyzed a selected mid-latitude area with small emission angles.

When one considers all of the branches, illustrated in Fig. 6b, this conclusion still stands. All of the individual branches appear to lie approximately along lines of constant modal ratios. It is also clear that there are large variations between the branches in relative mode 3 content, varying by at least a factor of 25. This range (25:1) of relative mode 3 concentration is a lower limit, arrived at by assuming that both the middle and lower clouds vary in modal concentration. If only lower cloud variations are responsible, then a much larger concentration range is indicated. At this stage of analysis, it is difficult to separate out the range of particle size variation from the altitude range over which this variation occurs. We can only conclude that large variations in the ratio of mode 3 to mode 2' occur in the lower levels of Venus's clouds. In some regions, these clouds are nearly pure mode 3, in other regions they are nearly pure mode 2'.

The spatial distribution of the branches, if interpreted as variations in mode 3 to mode 2' concentrations, implies that during the time of the Venus encounter the northern hemisphere consists of particles with larger mean radius, i.e. a higher mode 3/mode 2' ratio, than is generally found in the south. A deviation from this general rule occurs in a narrow linear band located at ~ 45 N. Compared to nearby regions, the particles here are much smaller in average size.

In proposing this explanation in terms of cloud particle size, we do not mean to imply that other explanations are not possible. In particular, variations in sulfuric acid concentration of the cloud particles might be envisioned. We have briefly examined this hypothesis by performing theoretical calculations for two extreme cases of sulfuric acid concentration, 75 % and 95% (by weight). We considered clouds of only mode 3 particles, for which absorption effects are the greatest, and compute radiances for various optical depths. The influence of sulfuric acid concentration on the absorption coefficient is small at 1.74 *pm*, decreasing by ~4 % as the concentration increases from 75 % to 95 % (Palmer and Williams, 1975). At 2.30 μm there is a factor of eight larger decrease. Radiative transfer calculations show that the net effect is to increase the 2.30 μm radiance by ~ 30 %. However, the observations show an increase of 125 % in the 2.30 μm radiance (for constant $I'_{1.74}$). Consequently, changes in sulfuric acid content can account for only about one quarter of the observed variation. Based upon the relatively narrow concentration range (+/- 5 %) suggested by Knollenberg and Hunten (1980), we submit that concentration changes are a minor effect in formation of the branches.

In addition to size and sulfuric acid content, there is the possibility that the large Mode 3 particles are not sulfuric acid droplets at all, but are in fact solid particles of unknown compositions (Knollenberg and Hun ten, 1980). Our wavelength coverage is insufficient to provide any information or constraints regarding this possibility. We can only note that our results are consistent with sulfuric acid cloud particles of varying sizes.

One might also consider the effect of varying the temperature in the lower atmosphere, which will affect $I_{1.74}$ more than $I_{2.30}$ because of the lower depth of formation of the former. We feel that it is unlikely that this sort of explanation can be the sole cause of the observed

branches, since their spatial structure is closely correlated to cloud features, which rotate at a much faster rate than the deep atmosphere. However, it is conceivable that some larger-scale features less obviously connected with the clouds might be due to such an effect; e.g., the asymmetry between the northern and southern hemispheres in Fig.4a.

CONCLUSIONS AND SPECULATIONS

We have investigated the correlation of 1.74 μm and 2.30pm radiation transmitted through the Venus clouds. These data cluster into distinct branches which we interpret as regions of distinct and different mixes of small and large particles (Modes 2' and 3). There is a tendency for more large particles in the northern hemisphere, although this may not be representative of the average situation. The spatial scale for a particular concentration (branch) is quite large, at least during the instance of the *Galileo* flyby. It is natural to assume different origins for these differently-sized particles, and that formation of the modes 2' and 3 particles occur in different altitude regimes (e.g. photochemical processes near the cloud tops and condensation near the bottom of the clouds). The observed mixtures of these modes -the branches - might therefore indicate mixing of air parcels between these two vertically stratified source regions. However, the large horizontal scales of this constant- mixing-ratio behavior is surprising, and far different from terrestrial examples, where horizontal mixing scales are only a few times the local scale height.

ACKNOWLEDGEMENT

It is a pleasure to acknowledge the assistance of Rober Mehlman. Portions of this work were performed at the Jet Propulsion Laboratory, California Institute of Technology, under a contract with the National Aeronautics and Space Administration.

REFERENCES

Allen, D.A. and J.W. Crawford (1984), Cloud structure on the dark side of Venus, *Nature* 307, 222-224.

Carlson, R. W., P.R. Weissman, W.D. Smythe, J.C. Mahoney and the NIMS Science and Engineering Teams (1992), Near-infrared mapping spectrometer experiment on Galileo, *Sp. Sci. Rev. 60,* 457-502.

Carlson, R.W., K.H. Baines, T. Encrenaz, F.W. Taylor, P. Drossart, L.W. Kamp, J.B. Pollack, E. Lellouch, A.D. Collard, S.B. Calcutt, D.H. Grinspoon, P.R. Weissman, W.D. Smythe, A.C. Ocampo, G.E. Danielson, F.P. Fanale, T.V. Johnson, H.H. Kieffer, D.L. Matson, T.B. McCord and L.A. Soderblom (1991), Galileo infrared imaging spectrometer measurements at Venus, *Science 253, 1541-1548.*

Crisp, D., W. M. Sinton, K. W. Hodapp, B. Ragent, F. Gerbault, J. H. Goebel, R. G. Probst, D. A. Allen, K. Pierce and K. R. Stapelfeldt (1989), The nature of the near-infrared features on the Venus night side, *Science 246, 506-509.*

Esposito, L. W., R.G. Knollenberg, M.Ya. Marov, O.B. Toon, and R.P. Turco (1983), The clouds and hazes on Venus, in *Venus* (Eds. D.M. Hunten, L. Colin, T.M. Donahue and V.I. Moroz) Univ. Arizona Press.

Grinspoon, D. H., J.B. Pollack, B.R. Sitton, R.W. Carlson, L.W. Kamp, K.H. Baines, T. Encrenaz and F. W. Taylor (1993), Probing Venus' cloud structure with Galileo NIMS, *Planet. Sp. Sci.* this issue.

Kamp, L. W. and F. W. Taylor (1990), Radiative transfer models of the nightside of Venus, *Icarus 86, 510-529.*

Knollenberg, R.G. and D.M. Hunten (1979), Clouds of Venus: particle size distribution measurements, *Science 203, 792-795.*

Knollenberg, R.G. and D.M. Hunten (1980), the microphysics of the clouds of Venus: results of the Pioneer Venus particle size spectrometer experiment, J. *Geophys. Res. 85,* 8039-8058.

Marov, M. Ya, V. E. Lystsev, V. N. Lebedev, N. L. Lukashevich and V. P. Shari (1980), The structure and microphysical properties of the Venus clouds: *Venera* 9, 10, *and 11* data, *Icarus 44, 608-639.*

Moshkin, B. E., V. I. Moroz, V. 1. Gnedykh, A. V. Grigor'ev, L. V. Zasova and A. P. Ekonomov (1986), *Vega 1,* 2 optical spectrometry of Venus atmospheric aerosols at the 60-30 km levels: preliminary results, Sov. *Aston. Lett 12, 36-39.*

Palmer, K.F. and D. Williams (1975), Optical constants of sulfuric acid; application to the clouds of Venus ?, *Appl. Optics 14, 208-219.*

Pollack, J.B., J.B. Dalton, D.H. Grinspoon, R. Wattson, R. Freedman, D. Crisp, D. Allen, B. Bezard, C. deBergh, L.P. Giver, Q. Ma, and R. Tipping (1993), Near-infrared light from Venus' nightside: a spectroscopic analysis, *Icarus,* in press.

Ragent, B., and J. Blamont (1980), The structure of the clouds of Venus: results of the Pioneer Venus nephelometer experiment, *J. Geophys. Res.* 85, 8089-8105.

Roos, M., P. Drossart, Th. Encrenaz, E. Lellouch and B. Bezard (1993), The upper clouds of Venus: determination of the scale height from NIMS-Galileo infrared data, *Planet. Space. Sci.* this issue.

Rossow, W. B., A.D. Del Genie, S.S. Limaye, and L.D. Travis (1980), Cloud morphology and motions from Pioneer Venus images, *J. Geophys. Res.* 85, 8107-8128.

Schinder, P.J., P.J. Gierasch, S.S. Leroy and M.D. Smith (1990), Waves, advection, and cloud patterns on Venus, *J. Atmos. Sci. 47, 2037-2052.*

FIGURE CAPTIONS

Fig. 1. Theoretical and observed limb darkening. Data and theoretical results for 2.30pm and 1.74 μm radiation are shown in (A) and (B) respectively. The radiances I are plotted as a function of the cosine of the emission angle θ_e. The upper boundary of the data, which have been normalized at θ_e = O, agrees well with the theoretically predicted limb darkening, shown as the solid curve. The accuracy of the theoretical curves at high emission angles are suspect due to the sphericity of the atmosphere. The dashed line is a linear approximation to the theoretical curve.

Fig. 2. Scatter diagram for emission angle corrected radiances. Two representations of the same data are shown; linear scales are used in (A) and logarithmic scales in (B). Each point represents a pixel and gives the corresponding corrected radiances at 2.30 μm and 1.74 μm, $(I'_{2.30}, I'_{1.74})$. The data follow distinct tracks and visual examination suggests that there are four or more of these different branches. Further analysis shows at least one more, and these branches are enumerated *in* A.

Fig. 3. Histograms of the branching parameter, *D*. The bin value is proportional to *D*, the logarithmic distance from a reference line running through the center of the data of Fig. 2b. Peaks in the histogram correspond to the branches indicated in Fig. 1. The upper panel uses data from the upper one third of the observed disc, while the bottom panel uses data from the bottom two-thirds. Extreme emission angles have been excluded. Branch number 2 may consist of two separate branches, and the fifth branch may also be a composite of overlapping branches,

Fig. 4. Venus cloud maps. (A) a map of the branching parameter which we interpret here as being related to particle size and the mix of mode 2' and mode 3 particles. This false color image uses 32 colors, with high values of the branching parameter shown as magenta, progressing to blue for small values. If interpreted in terms of mean particle size, red corresponds to large particles (i.e. a large mode 3 to mode 2' ratio) while green/blue indicates the converse. (B) A 2.30 μm image, uncorrected for emission angle. Note the correlation between this image and A, particularly in the southern hemisphere. In this, and the other images, the black pixels are generally due to spacecraft obscuration. (C) Cloud top thermal emission image obtained at a wavelength of 4.56 μm. (D) A repeat of the image in A along with a reference grid. West longitude values are given.

Fig, 5. Theoretical radiances for three cloud cases. The 1.74 and 2.3 μm radiances are computed for three cases: A cloud of only mode 2' particles, a cloud of only mode 3 particles, and an intermediate case, with roughly equal 2.30 opacities for both modes. Note the similarity of the shapes of these curves with the scatter plot of Fig. la.

Fig. 6. Theoretical and observed radiances. Four theoretical curves are shown. For each curve, the ratio of mode 3 to mode 2' content is constant and the total opacity of the lower cloud is varied. The central curve is for a nominal cloud model while curves lying above and below correspond to relative enhancement or depletion of relative mode 3 content. In (A) we compare these theoretical curves to the scatter plot for Branch number 3. Note that the slope of the run of these data is nearly identical to the theoretical curves, indicating a relatively constant modal ratio for this branch. In (B) we compare the curves to the composite scatter plot of Fig. lb. The dispersion of these branches indicates that large variations in the modal ratio occurs among the different branches.

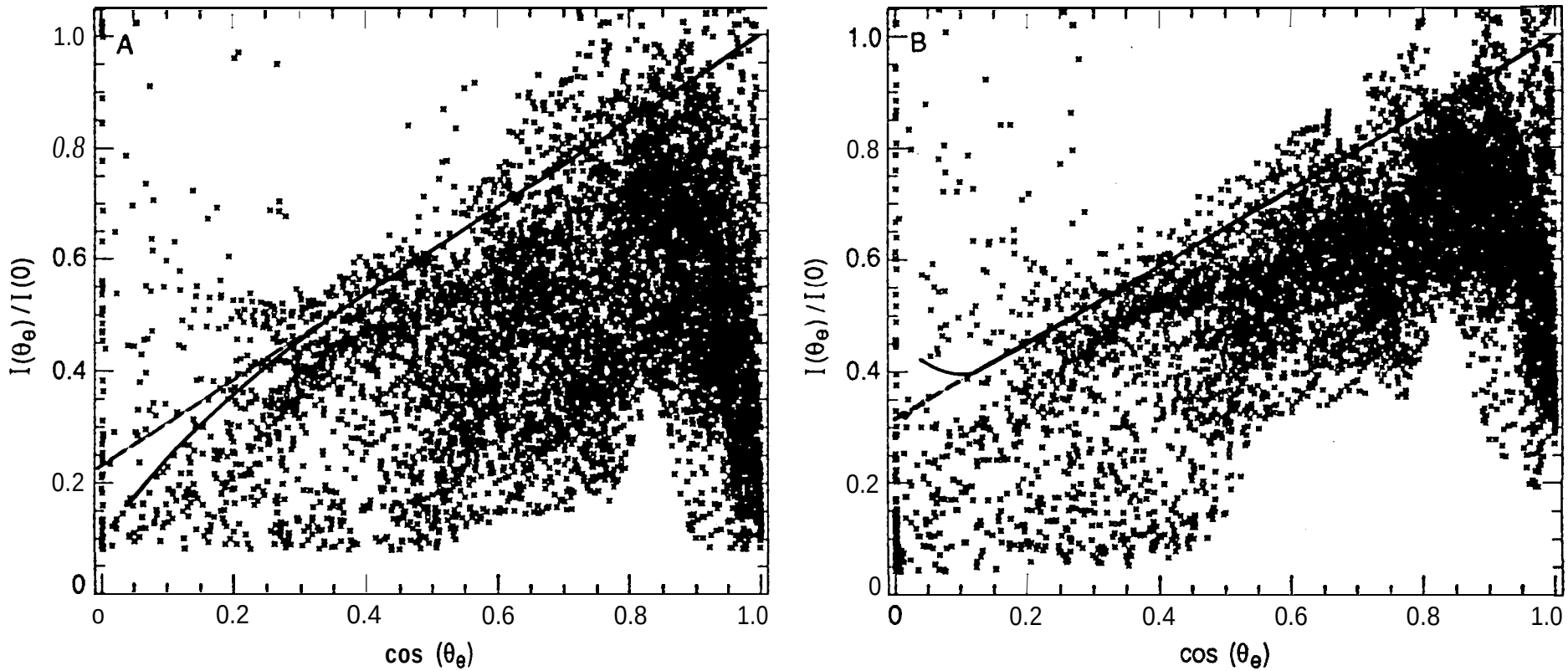

Fig. 1

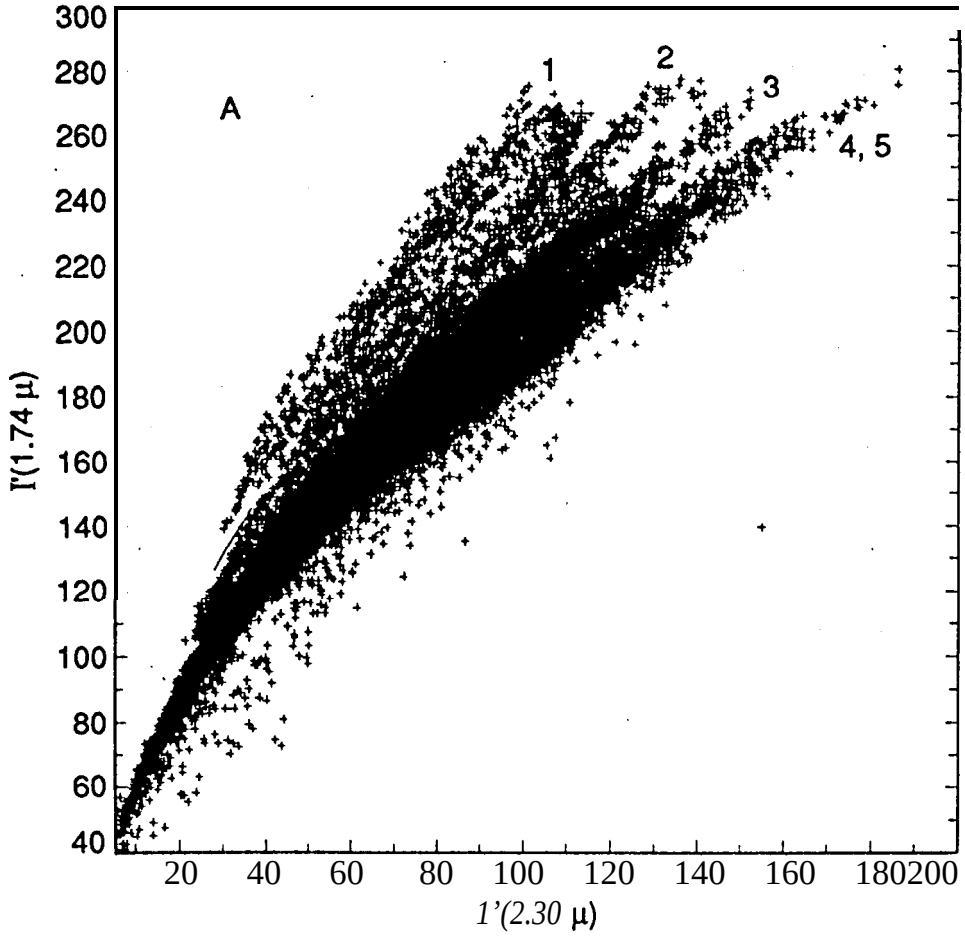
A
1
2
3
4, 5
300
280
260
240
220
200
180
160
140
120
100
80
60
40
Γ(1.74 μ)
20
40
60
80
100
120
140
160
180200
1'(2.30 μ)

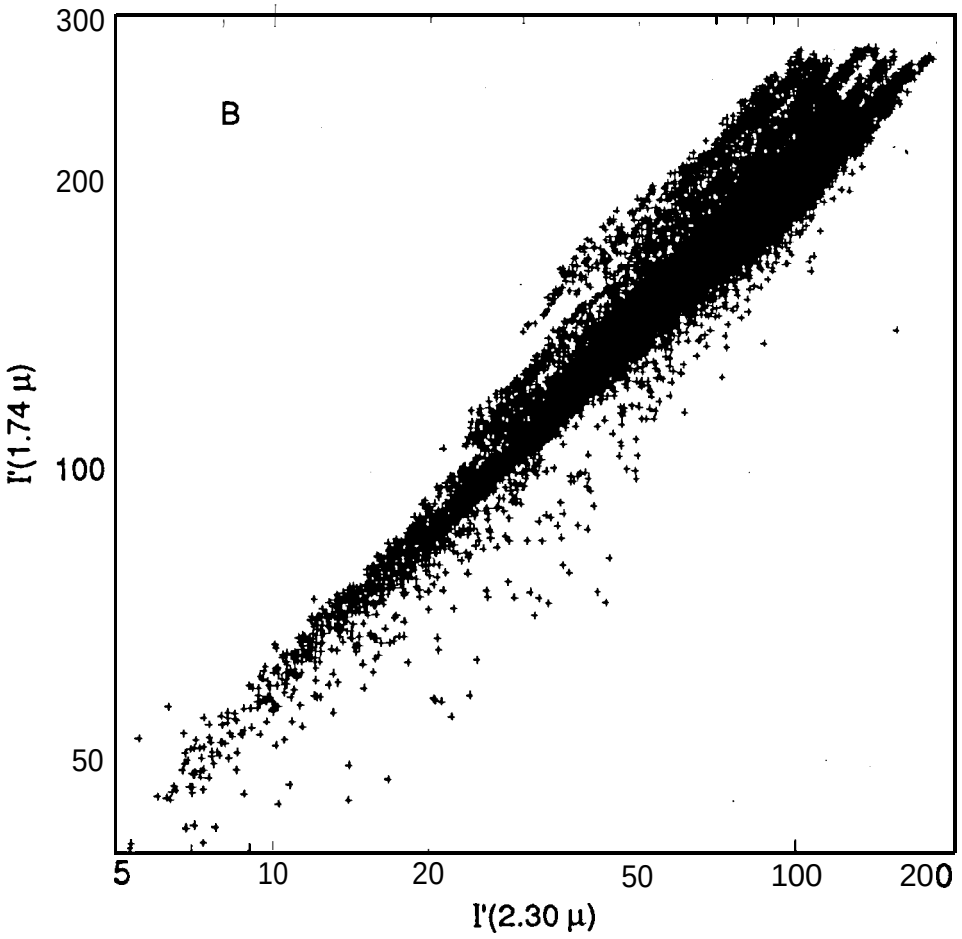
B
300
200
100
50
Γ(1.74 μ)
5
10
20
50
100
200
I'(2.30 μ)

Fig. 2

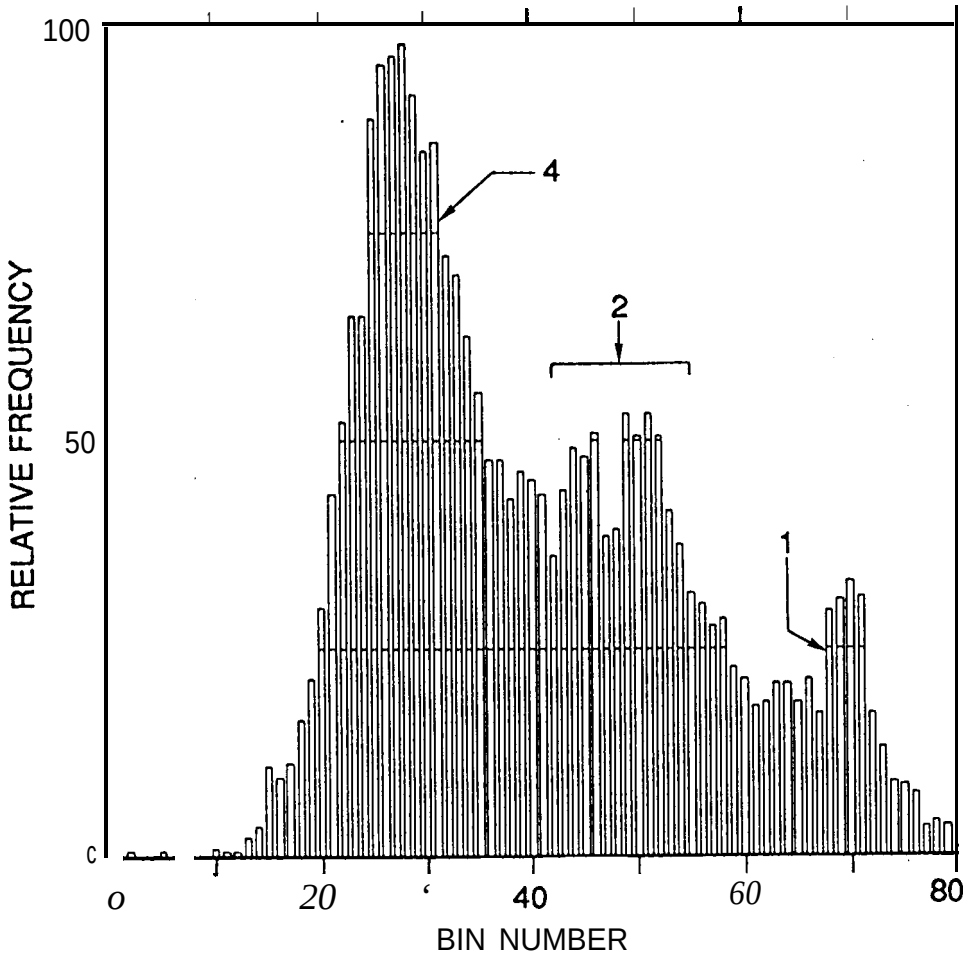
100
50
0
RELATIVE FREQUENCY
4
2
1
0
20
40
60
80
BIN NUMBER

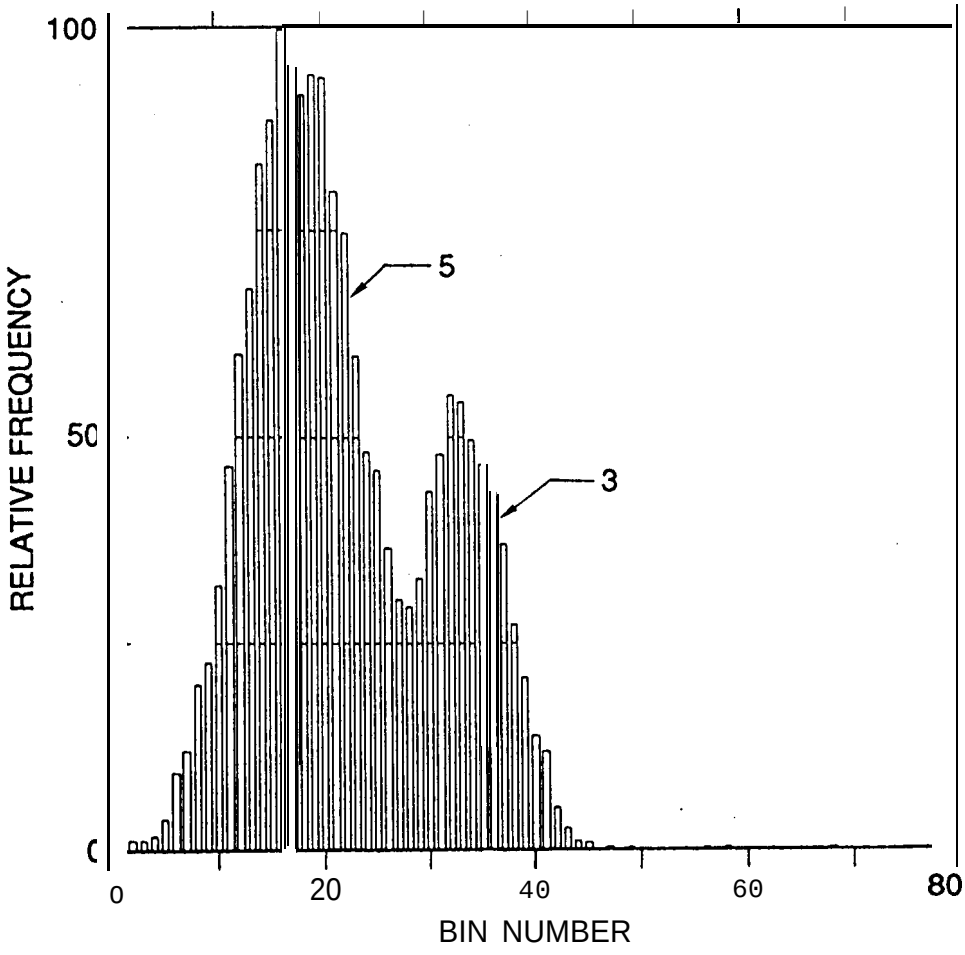
100
50
0
RELATIVE FREQUENCY
5
3
0
20
40
60
80
BIN NUMBER

Fig. 3

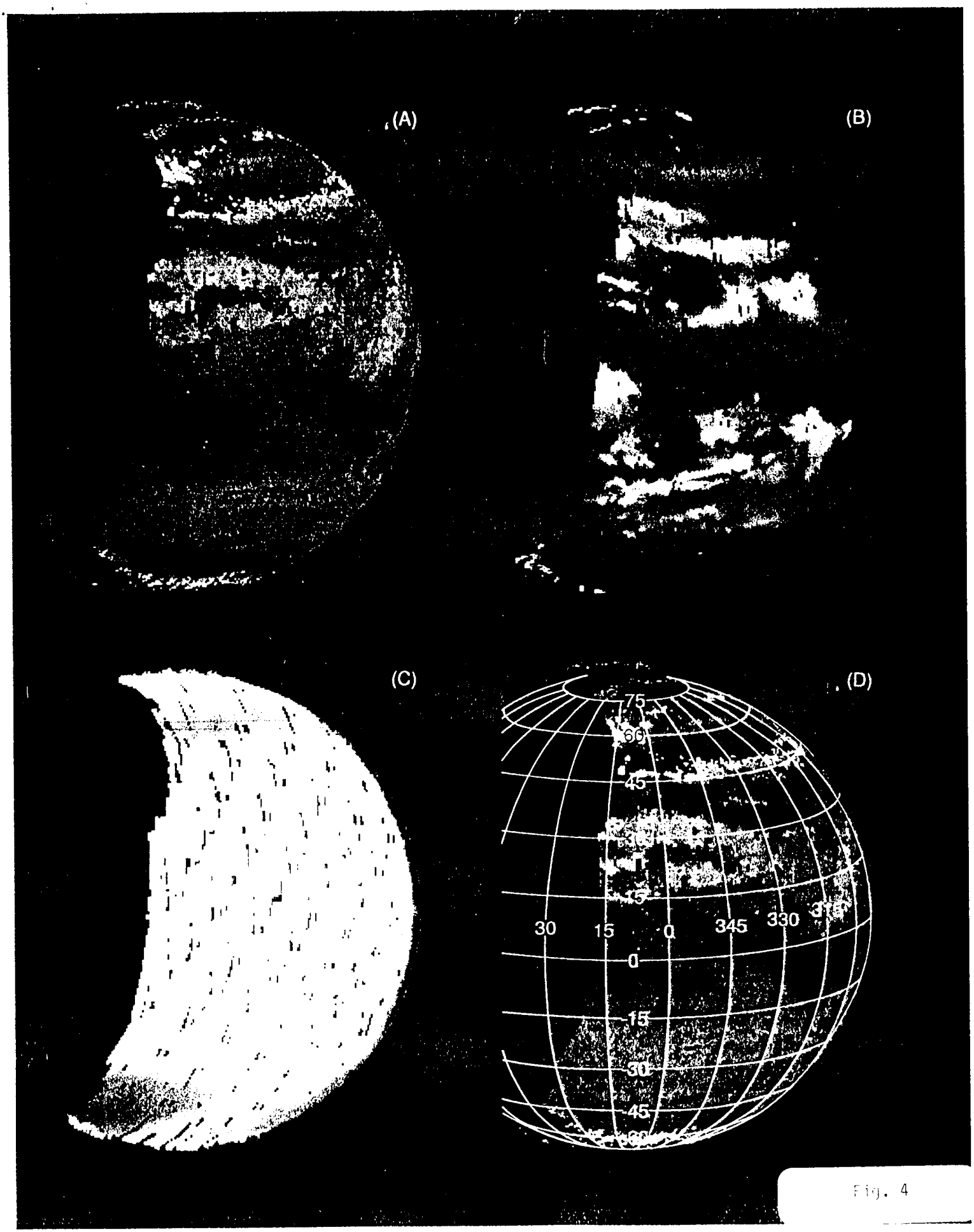

Fig. 4

[redacted]

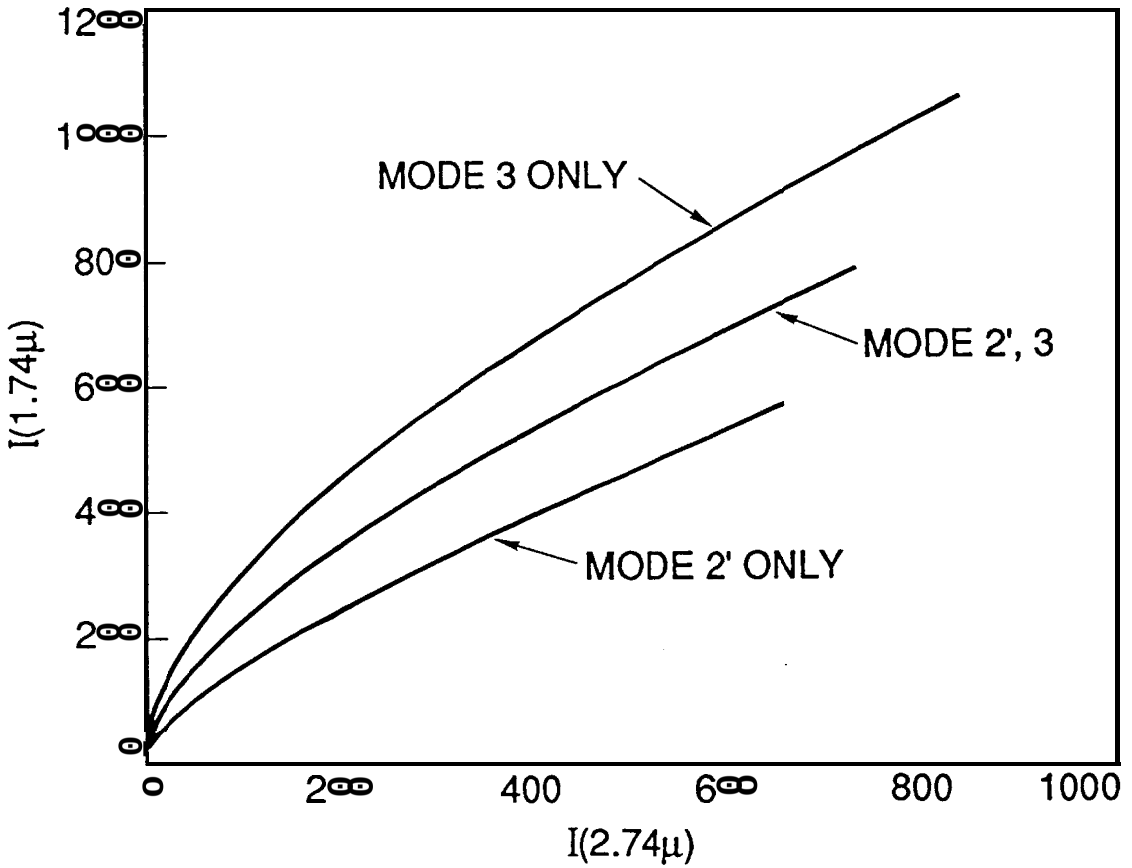
1200
1000
800
600
400
200
0
I(1.74μ)
MODE 3 ONLY
MODE 2', 3
MODE 2' ONLY
0
200
400
600
800
1000
I(2.74μ)

Fig. 5

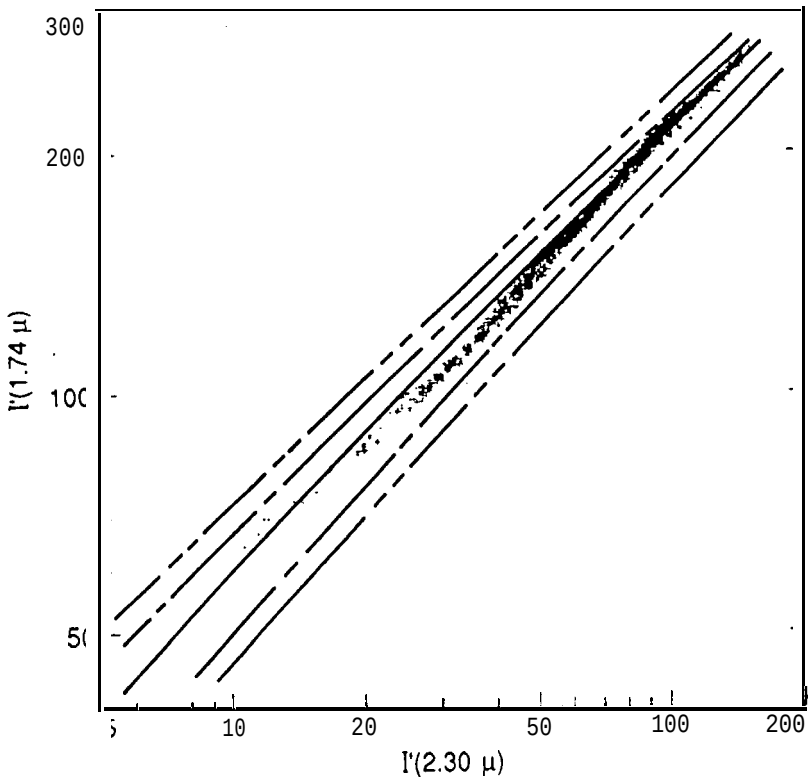
300
200
I'(1.74 μ)
10
20
50
100
200
I'(2.30 μ)

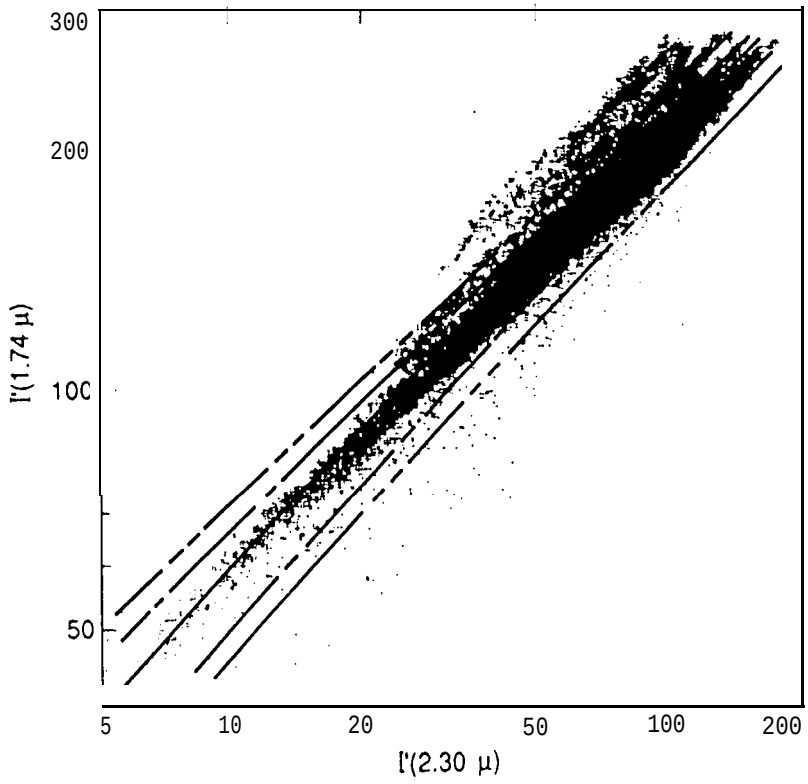
300
200
I'(1.74 μ)
50
5
10
20
50
100
200
I'(2.30 μ)

Fig. 6